

A sensitivity analysis of a mathematical model for the synergistic interplay of Amyloid beta and tau on the dynamics of Alzheimer's disease

Michiel Bertsch^{1,2}, Bruno Franchi³, Valentina Meschini¹, Maria Carla Tesi³, and Andrea Tosin⁴

¹Department of Mathematics, University of Roma "Tor Vergata", Roma, Italy

²Istituto per le Applicazioni del Calcolo "M. Picone", Consiglio Nazionale delle Ricerche, Roma, Italy

³Department of Mathematics, University of Bologna, Bologna, Italy

⁴Department of Mathematical Sciences "G. L. Lagrange", Politecnico di Torino, Torino, Italy

Abstract

We propose a mathematical model for the onset and progression of Alzheimer's disease based on transport and diffusion equations. We treat brain neurons as a continuous medium and structure them by their degree of malfunctioning. Three different mechanisms are assumed to be relevant for the temporal evolution of the disease: i) diffusion and agglomeration of soluble Amyloid beta, ii) effects of phosphorylated tau protein and iii) neuron-to-neuron prion-like transmission of the disease. We model these processes by a system of Smoluchowski equations for the Amyloid beta concentration, an evolution equation for the dynamics of tau protein and a kinetic-type transport equation for the distribution function of the degree of malfunctioning of neurons. The latter equation contains an integral term describing the random onset of the disease as a jump process localized in particularly sensitive areas of the brain. We are particularly interested in investigating the effects of the synergistic interplay of Amyloid beta and tau on the dynamics of Alzheimer's disease. The output of our numerical simulations, although in 2D with an over-simplified geometry, is in good qualitative agreement with clinical findings concerning both the disease distribution in the brain, which varies from early to advanced stages, and the effects of tau on the dynamics of the disease.

Keywords: Alzheimer's disease, transport and diffusion equations, Smoluchowski equations, numerical simulations

Mathematics Subject Classification: 35M13, 35Q92, 92B99.

1 Introduction

Alzheimer's disease (AD) is a progressive neurodegenerative disease characterized by the formation of insoluble protein aggregates and loss of neurons and synapses. This causes a progressive decline in memory and other cognitive functions, and ultimately dementia. The processes leading to protein aggregation and neurodegeneration are only partially understood [1]. AD was first described in 1907 by Alois Alzheimer who reported two pathological hallmarks in the brain: amyloid plaques in the extracellular medium and neurofibrillary tangles (NFTs) inside neurons. It was not until eight decades later that the major proteinaceous components of these lesions were identified. Amyloid plaques consist primarily of aggregates of Amyloid beta peptides ($A\beta$) [8], whereas the main constituent of neurofibrillary tangles is tau protein (τ) in a hyperphosphorylated form [10]. Up to now, $A\beta$ and τ remain the major therapeutic targets for the treatment of AD. According to the 2019 World Alzheimer Report, it is estimated that there are presently 50 million people living with AD and related disorders, and this figure is expected to increase to 152 million by 2050 due to

an increasingly aged population. As current treatments are purely for modest symptomatic relief, there is an urgent need for reliable and efficient computational models able to provide insights for effective therapies for the disease.

How $A\beta$ and τ interact to cause neurodegeneration remains a major knowledge gap in the field. There is substantial evidence that oligomeric $A\beta$ has a role in synapse degeneration, both in computational models and in human postmortem tissues, and that pathological forms of τ are sufficient to induce synapse loss and circuit dysfunction in models of tauopathy. But there is also increasing evidence that the progression of AD dementia is driven by the synergistic interaction between $A\beta$ and τ , which is responsible for synaptic dysfunction, neurofibrillary tangle mediated neuron loss, and behavioral deficits [22, 17, 7].

1.1 Amyloid β

Sequential cleavage of the amyloid precursor protein (APP) by β - and γ -secretase results in the generation of a range of $A\beta$ peptides from 39 to 43 amino acid residues in length, although $A\beta_{40}$ and $A\beta_{42}$ are the predominant species in vivo. The hydrophobic nature of the peptides, particularly $A\beta_{42}$ and $A\beta_{43}$, allows them to self-aggregate and form a myriad of species from dimers to small molecular weight oligomers, to protofibrils, to fibrils, ultimately leading to their deposition as amyloid plaques. Furthermore, $A\beta$ peptides can also undergo pyroglutamate modification at amino acid position three ($A\beta_{3(pE)}$); this increases the stability, aggregation propensity and neurotoxicity compared to full-length, unmodified $A\beta$. The mechanism by which excessive $A\beta$ accumulation occurs in sporadic AD remains unclear. Reduced $A\beta$ clearance or small increases in $A\beta$ production over a long period of time are potential mechanisms that result in the accumulation of $A\beta$ in the brain. There is considerable debate regarding which of the $A\beta$ species is most neurotoxic. Increasing evidence suggests that small molecular weight oligomers correlate best with the disease and that insoluble amyloid plaques are not toxic [19]. It seems that the most toxic $A\beta$ is identified in $A\beta_{42}$.

1.2 The microtubule-associated τ

The τ protein is a microtubule-associated protein (MAP) that is encoded by the MAPT gene. The protein contains an amino-terminal projection domain, a proline-rich region, a carboxy-terminal domain with microtubule-binding repeats, and a short tail sequence. Tau has been reported to interact with many proteins, serving important scaffolding functions [16]. In particular, it acts in concert with heterodimers of α - and β -tubulin to assemble microtubules and regulate motor-driven axonal transport. In the adult human brain τ occurs in six isoforms, with either three or four microtubule-binding domains, which result from alternative splicing of exons 2, 3 and 10 of the MAPT gene. Tau is enriched inside the neurons. In nature neurons it is largely found in axons; in dendrites it is present in smaller amounts. The distinguishing factor that separates normal τ from that observed in patients with AD is its hyperphosphorylation. The longest isoforms of human τ contain 80 serine and threonine residues and five tyrosine residues, all of which can potentially be phosphorylated. In the disease state, the amount of hyperphosphorylated τ is at least three times higher than that in the normal brain [14]. It is not entirely clear, however, whether phosphorylation of τ at specific sites results in the pathogenicity observed in AD or whether it only requires a certain overall level of phosphorylation. Nevertheless, hyperphosphorylation of τ negatively regulates the binding of τ to microtubules, which compromises microtubule stabilization and axonal transport. Hyperphosphorylation also increases the capacity of τ to self-assemble and form aggregates from oligomers to fibrils, eventually leading to its deposition as NFTs. In addition, hyperphosphorylated τ has been shown to interfere with neuronal functions, causing reduced mitochondrial respiration, altered mitochondrial dynamics and impaired axonal transport. Tau pathology progresses through distinct neural networks, and in AD NFTs are prominent in the cortex in an early stage, and later appear in anatomically connected brain regions.

Furthermore, it has been demonstrated that excess τ aggregates can be released into the extracellular medium, to be internalized by surrounding neurons and induce the fibrillization of

endogenous τ ; this suggests a role for τ seeding in neurodegeneration [11].

1.3 Aims of the model

Increasing clinical evidence suggests that $A\beta$ and τ do not act in isolation and that there is significant crosstalk between these two molecules [18]. Experiments using primary neurons or neuronal cell lines have shown that application of $A\beta$ oligomers increases τ phosphorylation [21]. This suggests a link between $A\beta$ toxicity and τ pathology, but it is unclear how $A\beta$ and τ interact in pathological cases. Often τ is placed downstream of $A\beta$ in a pathocascade, providing support for the amyloid cascade hypothesis [9]. Having these considerations in mind the main purpose of the present paper is to provide a reliable mathematical tool for better investigating mutual interaction mechanisms between $A\beta$ and τ and assess the resulting effect on the dynamics of Alzheimer's disease. In this context we present a multiscale model for the onset and evolution of AD which accounts for the diffusion and agglomeration of $A\beta$ peptide, the protein τ and the spreading of the disease. We stress that different spatial and temporal scales are needed to capture the complex dynamics of AD in a single model: microscopic spatial scales to describe the role of the neurons, macroscopic spatial and short temporal (minutes, hours) scales for the description of relevant diffusion processes in the brain, and large temporal scales (years, decades) for the description of the global evolution of AD.

2 The mathematical model

The mathematical model employed in the present study derives from that extensively described, analyzed and motivated in [2, 4, 5]. Modifications to the original model are made to cope with the main focus of the present study: the interplay between $A\beta$ and τ .

We identify a portion of cerebral tissue by an either two- or three-dimensional bounded set Ω . The space variable is denoted by x . Two time scales are needed to describe the evolution of the disease over a period of years: a short (i.e., rapid) s -scale, where the unit time coincides with hours, for the diffusion and agglomeration of $A\beta$ [16]; and a long (i.e., slow) t -scale, where the unit time coincides with several months, for the progression of AD. Introducing a small constant $0 < \varepsilon \ll 1$, the relationship between these two time scales can be expressed as

$$t = \varepsilon s. \quad (1)$$

On the whole, the model that we propose for the present study reads as follows:

$$\begin{cases} \partial_t f + \partial_a(fv[f]) = J[f] & \text{in } \Omega \times [0, 1] \times (0, T] & (2a) \\ \varepsilon \partial_t u_1 - d_1 \Delta u_1 = -\alpha u_1 U + \mathcal{F}[f] - \sigma_1 u_1 & \text{in } Q_T = \Omega \times (0, T] & (2b) \\ \varepsilon \partial_t u_2 - d_2 \Delta u_2 = \frac{\alpha}{2} u_1^2 - \alpha u_2 U - \sigma_2 u_2 & \text{in } Q_T & (2c) \\ \varepsilon \partial_t u_3 = \frac{\alpha}{2} \sum_{3 \leq j+k < 6} u_j u_k & \text{in } Q_T & (2d) \\ \partial_t w = C_w(u_2 - U_w)^+ + \int_{\Omega} h_w(|y - x|)w(y, t) dy & \text{in } Q_T, & (2e) \end{cases}$$

where in (2b), (2c) we have set

$$U := \sum_{j=1}^3 u_j$$

for conciseness.

Equations (2b), (2c), (2d) are meant to describe the aggregation of $A\beta$. In particular, (2b) and (2c) are *compartmental* Smoluchowski-type equations with diffusion, agglomeration and cleavage. In particular:

- (i) $u_1(x, t)$ is the density of monomers in the point $x \in \Omega$ at time $t > 0$;
- (ii) $u_2(x, t)$ is the cumulative density of soluble oligomers, which are regarded collectively as a single compartment;
- (iii) $u_3(x, t)$ is the density of senile plaques.

Such a compartmental model, which in particular does not distinguish the densities of the soluble oligomers based on their length, is justified by the fact that, according to the literature, there is no clinical evidence on the maximum length of toxic oligomers [12]. Therefore, any precise value of such a length would be partly arbitrary. Although this may seem an over-simplification, in fact it is not because, as far as the results of the model are concerned, considering a more detailed description of the soluble oligomers with their precise lengths, such as e.g. in [2], has proved not to add significant information [3, 6]. The coefficient ε in front of the time derivatives is due to the relationship (1), in particular to the fact that, on the longer time scale t , the rate at which agglomeration and diffusion of $A\beta$ take place is as high as $\frac{1}{\varepsilon}$. Equation (2d) for the fibrils is written in the same spirit as the previous two ones, except for the fact that fibrils are assumed not to move. Thus the equation for their concentration u_3 does not feature a diffusion term. We include in this compartment all the combinations of monomers and oligomers producing $A\beta$ entities other than those comprised in the compartments 1 and 2, taking further into account that senile plaques do not aggregate with each other. Finally, consistently with the compartmental nature of the model, we take the coagulation parameters constant and equal to $\alpha > 0$, neglecting the fact that they may feature a dependence on the specific lengths of the aggregating oligomers, see [2].

Equation (2a) is instead a kinetic-type equation which describes the progression of the disease. Roughly speaking, $f = f(x, a, t)$ is the probability density of the degree of malfunctioning $a \in [0, 1]$ of neurons located in $x \in \Omega$ at time $t > 0$ and is such that $f(x, a, t) da$ represents the fraction of neurons in x which at time t have a degree of malfunctioning comprised between a and $a + da$. For a precise mathematical formulation in terms of probability measures, see [5]. We assume that a close to 0 stands for “the neuron is healthy” whereas a close to 1 stands for “the neuron is dead”.

The progression of AD occurs on the longer time scale t , over decades, and is determined by the deterioration rate $v[f] = v[f](x, a, t)$, which we assume to have the following form:

$$v[f](x, a, t) = C_G \int_0^1 (b - a)^+ f(x, b, t) db + C_S(1 - a)(u_2(x, t) - \bar{U})^+ + C_W(1 - a)w(x, t). \quad (3)$$

The integral term describes the propagation of AD among close neurons. The second term models instead the action of toxic $A\beta$ oligomers, leading ultimately to apoptosis. The threshold $\bar{U} > 0$ indicates the minimal amount of toxic $A\beta$ needed to damage neurons. Finally, $C_G, C_S > 0$ are proportionality constants. The third term accounts for the toxicity of the phosphorylated τ , whose density in the point $x \in \Omega$ at time $t > 0$ is denoted by $w(x, t)$. Specifically, this term assumes that such a toxicity is proportional to the concentration w through a proportionality constant $C_W > 0$ and that it is modulated by the current degree of malfunctioning of the neurons, in such a way that the more damaged the neurons the lower the impact of the toxic τ on them.

The term $J[f] = J[f](x, a, t)$ on the right-hand side of (2a) describes the possible random onset of AD in portions of the domain Ω as a result of a microscopic stochastic jump process. The latter takes into account the possibility that the degree of malfunctioning of neurons randomly jumps to higher values due to external agents or genetic factors. The explicit expression of this term is

$$J[f](x, a, t) = \eta \int_0^1 P(t, x, a_* \rightarrow a) f(x, a_*, t) da_* - f(x, a, t), \quad (4)$$

where $P(t, x, a_* \rightarrow a)$ denotes the probability that the degree of malfunctioning of neurons in the point $x \in \Omega$ jumps at time $t > 0$ from a_* to $a > a_*$. The coefficient $\eta > 0$ is the jump rate.

It is worth stressing that (2a), together with the detailed expressions (3), (4) of the terms $v[f]$, $J[f]$, may be obtained from a mesoscopic description of a microscopic model of neuron-to-neuron interactions as shown in [4].

Equation (2e) models the production and diffusion dynamics of the phosphorylated τ with density $w(x, t)$. Specifically, its production is linked to the presence of toxic $A\beta$ oligomers and furthermore its diffusion in the brain is assumed to happen according to a sort of prion-like mechanism. The first term on the right-hand side models the activation of the phosphorylated τ induced by toxic $A\beta$ oligomers, as soon as their concentration is above a certain threshold $U_w > 0$. If it is not, the phosphorylated τ is known not to activate [15]. The parameter $C_w > 0$ is a proportionality constant. The second term on the right-hand side describes the prion-like non-local spreading of the phosphorylated τ in possibly distant points of the brain according to the spatial kernel h_w . In the next Section 2.2 we will investigate in detail some properties of this integral term, which will further elucidate its physical meaning. We assume that the dynamics of τ take place on the slow time scale t . In the absence of precise indications from the biomedical literature, this choice seems reasonable in view of the fact that τ is especially involved in the progression of the disease rather than in the $A\beta$ agglomeration and the consequent formation of senile plaques.

To conclude the presentation of the model, we mention that the term $\mathcal{F}[f] = \mathcal{F}[f](x, a, t)$ in (2b) describes the production of $A\beta$ monomers by neurons, taking into account that, up to a certain extent, damaged neurons increase such a production. In view of these considerations, we choose

$$\mathcal{F}[f](x, a, t) = C_{\mathcal{F}} \int_0^1 (\mu_0 + a)(1 - a)f(x, a, t) da.$$

Here, the small constant $\mu_0 > 0$ accounts for $A\beta$ production by healthy neurons while the factor $1 - a$ expresses the fact that dead neurons do not produce amyloid. As usual, $C_{\mathcal{F}} > 0$ is a proportionality constant.

2.1 Initial and boundary conditions

As far as boundary conditions are concerned, we assume that $\partial\Omega$ consists of two smooth disjoint parts, say $\partial\Omega_0$ and $\partial\Omega_1$, being $\partial\Omega_0$ the outer boundary which delimits the considered portion of cerebral tissue and $\partial\Omega_1$ the inner boundary of the cerebral ventricles. On $\partial\Omega_0$ we prescribe classical no-flux conditions for all the concentrations. Conversely, on $\partial\Omega_1$ we prescribe a Robin condition for the concentrations of the $A\beta$ oligomer mimicking their removal by the cerebrospinal fluid through the choroid plexus [13, 20]. On the whole, we have then:

$$\begin{cases} \nabla u_i \cdot \mathbf{n} = 0 & \text{on } \partial\Omega_0, \ i = 1, 2 \\ \nabla u_i \cdot \mathbf{n} = -\beta u_i & \text{on } \partial\Omega_1, \ i = 1, 2 \\ \nabla w \cdot \mathbf{n} = 0 & \text{on } \partial\Omega, \end{cases} \quad (5)$$

where $\beta > 0$ is a proportionality parameter and \mathbf{n} the outward normal unit vector to $\partial\Omega$. We also complement system (2) with a proper set of initial conditions:

$$f(x, a, 0) = f_0(x, a), \quad u_i(x, 0) = u_{0,i}(x) \ (i = 1, 2, 3), \quad w(x, 0) = 0. \quad (6)$$

A numerical discretisation of the initial/boundary-valued problem (2)-(5)-(6) can be set up straightforwardly by adapting the one described in detail in [2].

2.2 Mathematical insights into the equation for τ

In this section, we want to explore the effect of the non-local term

$$I(x, t) := \int_{\Omega} h_w(|y - x|)w(y, t) dy$$

in (2e) with $\Omega \subset \mathbb{R}^n$ ($n = 2, 3$ from the physical point of view). Without loss of generality, we assume that the function $h_w : \mathbb{R}_+ \rightarrow \mathbb{R}_+$ is such that $h'_w(0^+) = 0$. Furthermore, we assume that h_w is compactly supported in $[0, R] \subset \mathbb{R}$, where $R > 0$ denotes the maximum distance at which the prion-like influence of the phosphorylated τ is supposed to be effective. Hence

$$I(x, t) = \int_{B_R(x)} h_w(|y - x|) w(y, t) dy.$$

Assume that R is sufficiently small, so that y is close to x , and that the functions h_w, w are smooth enough about 0^+ and x , respectively. By Taylor expansion we find:

$$\begin{aligned} h_w(|y - x|) &= h_w(0^+) + \frac{1}{2} h''_w(0^+) |y - x|^2 + o(|y - x|^2) \\ w(y, t) &= w(x, t) + \sum_{h=1}^n \partial_{x_h} w(x, t) (y_h - x_h) \\ &\quad + \frac{1}{2} \sum_{h,k=1}^n \partial_{x_h x_k}^2 w(x, t) (y_h - x_h) (y_k - x_k) + o(|y - x|^2), \end{aligned}$$

thus

$$\begin{aligned} h_w(|y - x|) w(y, t) &= h_w(0^+) w(x, t) + h_w(0^+) \sum_{h=1}^n \partial_{x_h} w(x, t) (y_h - x_h) \\ &\quad + \frac{1}{2} h_w(0^+) \sum_{h,k=1}^n \partial_{x_h x_k}^2 w(x, t) (y_h - x_h) (y_k - x_k) \\ &\quad + \frac{1}{2} h''_w(0^+) w(x, t) |y - x|^2 + o(|y - x|^2). \end{aligned}$$

Neglecting the remainder $o(|y - x|^2)$, we can therefore approximate $I(x, t)$ locally as

$$\begin{aligned} I(x, t) &\approx h_w(0^+) w(x, t) \int_{B_R(x)} dy + h_w(0^+) \sum_{h=1}^n \partial_{x_h} w(x, t) \int_{B_R(x)} (y_h - x_h) dy \\ &\quad + \frac{1}{2} h_w(0^+) \sum_{h,k=1}^n \partial_{x_h x_k}^2 w(x, t) \int_{B_R(x)} (y_h - x_h) (y_k - x_k) dy \\ &\quad + \frac{1}{2} h''_w(0^+) w(x, t) \int_{B_R(x)} |y - x|^2 dy. \end{aligned}$$

Let ω_n denote the volume of the unit ball in \mathbb{R}^n . By switching to polar coordinates, we find

$$\begin{aligned} \int_{B_R(x)} dy &= \omega_n R^n, \\ \int_{B_R(x)} (y_h - x_h) dy &= 0, \\ \int_{B_R(x)} (y_h - x_h) (y_k - x_k) dy &= \begin{cases} \frac{\omega_n}{n+2} R^{n+2} & \text{if } h = k \\ 0 & \text{if } h \neq k, \end{cases} \\ \int_{B_R(x)} |y - x|^2 dy &= \frac{n\omega_n}{n+2} R^{n+2}, \end{aligned}$$

whence finally

$$I(x, t) \approx \omega_n R^n \left(h_w(0^+) + \frac{n}{2(n+2)} h''_w(0^+) \right) w(x, t) + \frac{\omega_n R^{n+2}}{2(n+2)} h_w(0^+) \Delta w(x, t).$$

This shows that the local contribution of $I(x, t)$ to the spreading of the phosphorylated τ consists in a source term proportional to the quantity of τ already present in the site x and in a linear diffusion.

The local approximation of $I(x, t)$ elucidates also the role of the pointwise values of h_w, h_w'' in $r = 0$. If, for instance, we take

$$h_w(r) = \frac{1}{\omega_n R^n} \chi_{[0, R]}(r),$$

which makes $I(x, t)$ a uniform average of w in a neighbourhood of x of radius R , then $h_w(0^+) = \frac{1}{\omega_n R^n}$ and $h_w''(0^+) = 0$, whence

$$I(x, t) \approx w(x, t) + \frac{R^2}{2(n+2)} \Delta w(x, t).$$

This implies that, at the leading order in R , I consists in a pointwise source and, at higher order, in a diffusion term responsible for the spatial spreading of the phosphorylated τ .

3 Numerical results

In this section we present and discuss the numerical results of the mathematical model for Alzheimer's disease described in Section 2. We show the evolution of AD in two different modeling schemes: the first does not take into account the role of τ , whereas the second includes τ . We show spatial plots of the evolution of the disease, expressed by the quantity f in (2a), as well as spatial plots of the concentration of the toxic polymers, plaques and (phosphorylated) τ .

As a consequence of the compartmental description of the $A\beta$ oligomers, we find that the numerical results are quite sensitive to the constant \bar{U} in (3), which we will therefore tune accurately so as to observe in practice an evolution of the disease. In particular, a too high value of \bar{U} may easily hinder the effective toxicity of the cumulative density u_2 of $A\beta$, thereby preventing the occurrence of the dynamics of AD. As a matter of fact, since the phosphorylated τ contributes to the overall toxicity [17], the spread of the disease may also occur for a relatively high value of \bar{U} . In order to compare our numerical results corresponding to the two set-ups with and without τ , we test different cases with $\bar{U} = 0.01$ and $\bar{U} = 0.1$.

Besides \bar{U} , the equation for τ (see (2e)) contains another threshold constant U_w to which our model results very sensitive, since, out of a small range around $U_w = 0.01$, the numerical simulations suggest that the interaction between $A\beta$ and τ is not significant for the evolution of the disease.. Indeed, below $U_w = 0.01$ τ is excessively predominant, whereas, above the same order of magnitude the phosphorylation process is not triggered. Thus in all our simulations we keep U_w fixed, taking $U_w = 0.01$. In both simulation set-ups (with and without τ) we decide to carry out a sort of sensitivity analysis of the model outcomes to some parameters which we identify as representative and in particular with clinical implications. First of all, we consider the constant β , which enters the model through condition (5) at the boundary of the cerebral ventricles. Small values of β correspond to the assumption that a small amount of $A\beta$ is removed from the CSF through the choroid plexus. To test the sensitivity of the outcomes, we take for β two values: $\beta = 0.01$ and $\beta = 1$. Successively, another significant parameter is α (the coagulation parameter in (2b), (2c)). We decide to set α at different order of magnitude to observe how it affects the dynamics of $A\beta$ in the brain. We run a simulations campaign (both with and without inclusion of τ) varying α, β and \bar{U} but keeping fixed all the other parameters (see the captions in the sequel) which chosen values are reported in Table 1. We wish to point out that these values represent an order of magnitude and have a proper unit measure that can be deduced from the equations in which they are involved.

In Table 2 we give a schematic and complete overview of all the cases that have been tested in numerical simulations. Based on the resulting outcomes concerning how parameters and τ inclusion affect the overall dynamics of the disease, we aim to obtain insights on the disease, hopefully with applications to treatments and clinical procedures.

Table 1: Values of the fixed parameters

C_G	C_S	D	$\bar{\sigma}$	μ_0	C_F	C_W	\bar{U}_w
10^{-1}	10^{-3}	10^{-2}	1	10^{-2}	10	10	10^{-2}

Table 2: All the simulated cases and involved parameters with respective values

	Inclusion of τ	α	β	\bar{U}
Case 1	No	10	1	10^{-2}
Case 1.1	No	10	1	10^{-1}
Case 2	Yes	10	1	10^{-2}
Case 2.1	Yes	10	10^{-2}	10^{-2}
Case 2.2	Yes	1	1	10^{-2}
Case 2.3	Yes	10	1	10^{-1}

3.1 Case 1: $\alpha = 10$, $\beta = 1$ and no inclusion of τ (Figure 1)

The first case we simulate employs the same mathematical model for Alzheimer’s disease presented in [2] without τ in the model but, as mentioned above, assuming $N = 3$. As a consequence, the only toxic elements in the model are the dimers and the overall toxicity level is lower with respect to the same case in [2], in which $N = 50$. The toxicity level enters the formula for the degree of malfunctioning of the brain thus providing information on the health state of the brain. The parameter α , which regulates the coagulation of monomers and dimers, is taken equal to 10, while β , which refers to portion of toxic oligomers which is extracted from the brain, is equal to 1. As previously pointed out we choose the threshold value for the toxic u_2 equal to 10^{-2} which turns out to be with these set-up values the minimum order of magnitude to allow the disease to take place. The numerical outputs are shown in Figure 1, where the spatial plots of the degree of malfunctioning f at different times are plotted. The rectangle, which is the numerical domain, represents a two dimensional section of the brain where the upper part the frontal region, the lower part is the occipital region and the two inner rectangles are the ventricles. The disease starts from some random sources (the blue spot) and as time passes, owing to the neural infection, it propagates on other portions of the brain. It continues to spread until we reach a numerical equilibrium configuration in the sense that, even if we allow the time to increase, the spatial plot of f does not change. In this “stable” state we can see that there is a blue zone (dead part) but the brain is not completely ill. This result is clearly different from that obtained in [2], in which the whole brain is blue thus meaning basically that the patient is dead. The first question is: why does this happen in this case? The answer is that, having a coagulation factor $\alpha = 10$, the monomers aggregate to form dimers but remain briefly in this toxic state and then evolve to plaques, which are non toxic. Therefore the toxicity of the whole system is much lower. This is linked also to another question that is: why with this set-up the system reaches a “numerical steady state” that in [2] is not observed? This is because at a certain point the concentration of toxic oligomers u_2 goes below the threshold level, because toxic oligomers quickly agglomerate into plaques. This prevents the dynamics of the degree of malfunctioning from evolving further.

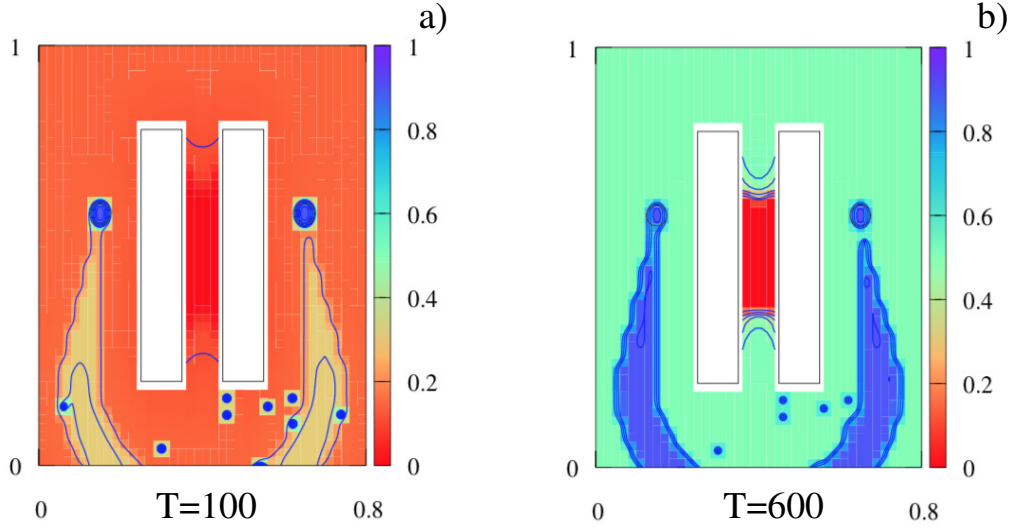


Figure 1: Spatial plots of the degree of malfunctioning of the brain for $\alpha = 10$, $\beta = 1$, $\bar{U} = 10^{-2}$ and without τ at two time instants: a) $T = 100$, b) $T = 600$

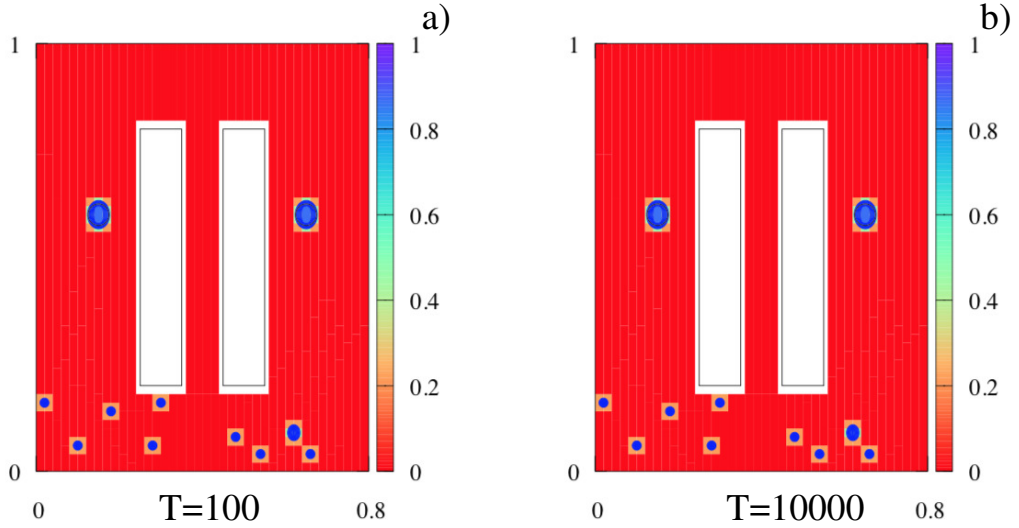


Figure 2: Spatial plots of the degree of malfunctioning of the brain for $\alpha = 10$, $\beta = 1$, $\bar{U} = 0.1$ and without τ at two time instants: a) $T=100$, b) $T=10000$.

3.2 Case 1.1: $\alpha = 10$, $\beta = 1$, no inclusion of τ and increased toxicity threshold (Figure 2)

The same numerical set-up of Case 1 of Table 1 is considered here, while increasing the value of \bar{U} to 0.1 to better investigate how this affects the system behaviour. We find that without the toxic effect induced by τ and with $\bar{U} = 10^{-1}$ the degree of malfunctioning of the brain does not evolve in time meaning that the disease is not able to spread, as shown in Figure 2.

3.3 Case 2: $\alpha = 10$, $\beta = 1$ and inclusion of τ (Figures 3, 4)

Here we exploit the novelty of this paper with respect to [2], since we include in the model the toxic effects of τ . All parameters are the same as in Case 1 of Table 1, i.e. we keep $\alpha = 10$,

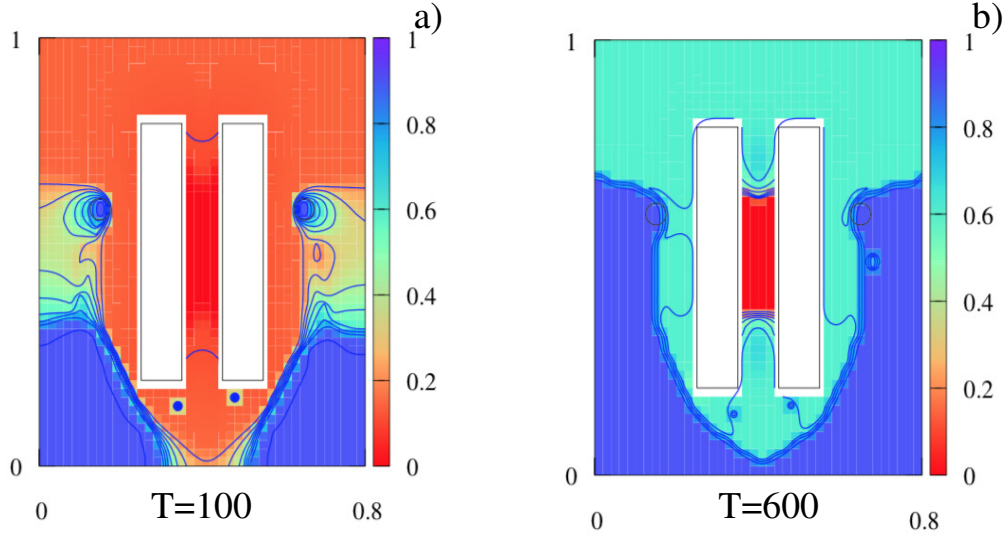


Figure 3: Spatial plots of the degree of malfunctioning of the brain for $\alpha = 10$, $\beta = 1$ and $\bar{U} = 0.01$ with τ at two times: a) $T=100$, b) $T=600$.

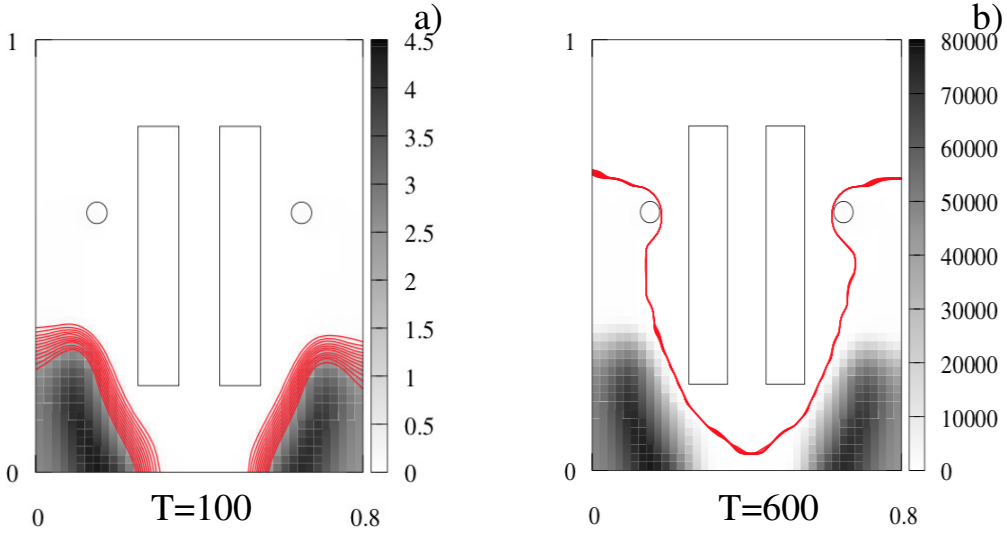


Figure 4: Spatial plots of τ for $\alpha = 10$, $\beta = 1$ and $\bar{U} = 0.01$ at two time instants: a) $T=100$, b) $T=600$.

$\beta = 1$ and $\bar{U} = 0.01$. In terms of the mathematical model we add an equation describing the diffusion in time of τ and also its toxic effects on the degree of malfunctioning of the brain as described in section 2.1. In figure 3 the spatial plots of the degree of malfunctioning of the brain show that a "numerical steady state" is reached. The dynamics is different from that of Case 1 since it starts as in Case 1 from some random sources but then evolves following the spreading trend of τ concentration. The evolution of the disease appears faster and the spatial localization of completely ill regions (the blue regions) is larger with respect to the disease dynamics analyzed in Case 1.

Also in this case we observe a sort of "localization" of Alzheimer's disease at the steady state. Looking at the spatial plots of f and τ (see Figures 3 and 4), the disease is not diffused in all the brain but only on a confined part of it. In fact, in this case the level of toxic oligomers u_2 goes below the threshold level $\bar{U} = 0.01$, thus avoiding the disease to continue spreading and damaging

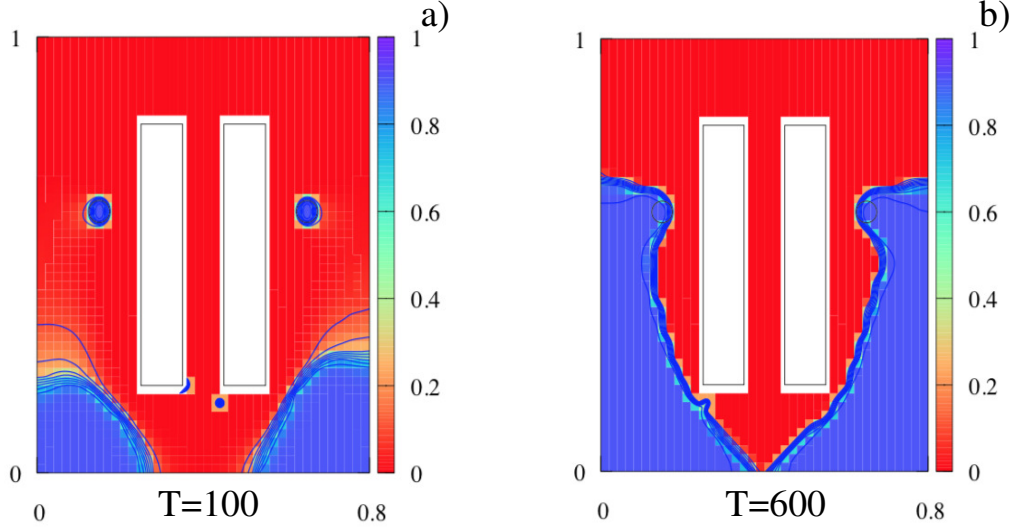


Figure 5: Spatial plots of the degree of malfunctioning of the brain for $\alpha = 10$, $\beta = 1$, $\bar{U} = 0.01$ and $C_G = 0$ at two times: a) $T=100$, b) $T=600$.

the whole brain.

3.3.1 Case 2*: $\alpha = 10$, $\beta = 1$, inclusion of τ and no neural infection (Figure 5)

In addition to what observed in Case 2 we aim to isolate the effects of the inclusion of τ on the numerical results. Thus we ignore the neuron-to-neuron infection mechanism, i.e we put the constant C_G of Section 2 equal to zero. We decide to select the same set-up of the parameters as in Case 2. The spatial plot of the degree of malfunctioning, shown in Figure 5, turns out to be different from that of Case 2 : the disease is less diffused in the cerebral parenchyma, and brain damages turn out to be localized in some specific portion of the brain in which τ is concentrated. Moreover, the brain is divided into two separated regions: the occipital part that is totally damaged (blue region) and the rest that is completely healthy (red region). In conclusion avoiding the prion-like infection mechanism between neurons strongly reduces the brain damages, thus underlying the higher toxic effects of synergistic interactions between $A\beta$ and τ when compared to their single toxic effects.

3.4 Case 2.1: $\alpha = 10$, $\beta = 0.01$ and inclusion of τ (Figures 6, 7)

In this simulation we use the same set of parameters values as in Case 2, except for the value of the parameter β that we set here equal to 0.01, meaning that less toxic oligomers are extracted from the brain with respect to Case 2. As for the cases described before we report in Figure 6 some snapshots of spatial plots of the degree of malfunctioning at two different instants. The overall dynamics of the spreading of the disease is similar to that described in Case 2, but the numerical steady state is reached faster and the completely damaged region of the brain is larger. This result appears reasonable since if less toxic elements are removed, then the degree of malfunctioning turns out to be higher. In agreement to what observed in Case 2, it is found that the spatial plots of the degree of malfunctioning reflects that of τ (see Figure 7). Indeed, τ in the present simulation is spread in a wider region.

3.5 Case 2.2: $\alpha = 1$, $\beta = 1$ and inclusion of τ (Figures 8, 9)

Here we use the same simulation set-up and parameters values as in Case 2, except for the coagulation parameter α that is set equal to 1. This means that the aggregation of monomers is slower

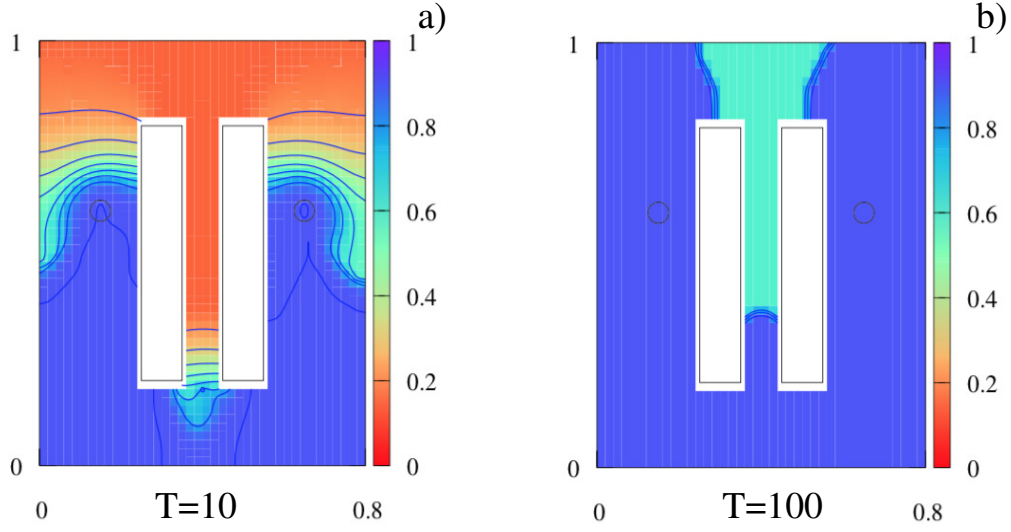


Figure 6: Spatial plots of the degree of malfunctioning for $\alpha = 10$, $\beta = 0.01$, $\bar{U} = 0.01$ and inclusion of τ at two times : a) $T=10$, b) $T=100$.

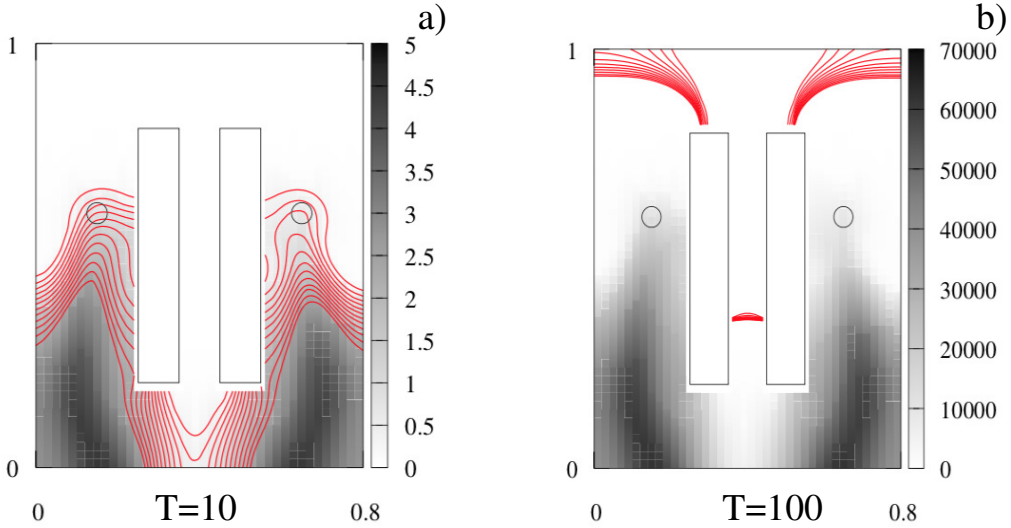


Figure 7: Spatial plots of τ for $\alpha = 10$, $\beta = 0.01$, $\bar{U} = 0.01$ at two time instants: a) $T=10$, b) $T=100$.

with respect to Case 2. The numerical outputs of this case are shown in Figure 8, where the spatial plots of the degree of malfunctioning of the brain are plotted at two different instants. Unlike all the cases seen so far, here the disease spreads faster into the whole cerebral parenchyma, until the brain is completely damaged. Moreover, looking at the spatial distribution of τ , see Figure 9, it is clear that, unlike the previous simulations, τ spreads very early on the whole brain, accelerating the spread of the disease and the complete damaging of the brain.

3.6 Case 2.3: $\alpha = 10$, $\beta = 1$, inclusion of τ and increased toxicity threshold (Figures 10, 11)

In all previous simulations the threshold value \bar{U} for the toxic oligomers u_2 remains constant and equals 0.01 which, as stressed in section 3, is the minimum value which allows the disease to start

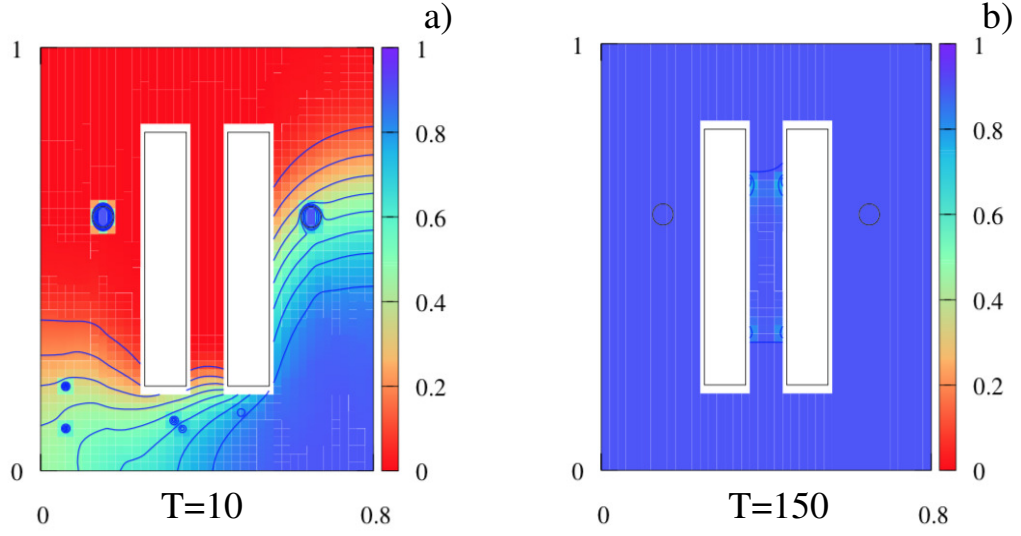


Figure 8: Spatial plots of the degree of malfunctioning for $\alpha = 1$, $\beta = 1$, $\bar{U} = 0.01$ and inculsion of τ at two times : a) $T=10$, b) $T=150$.

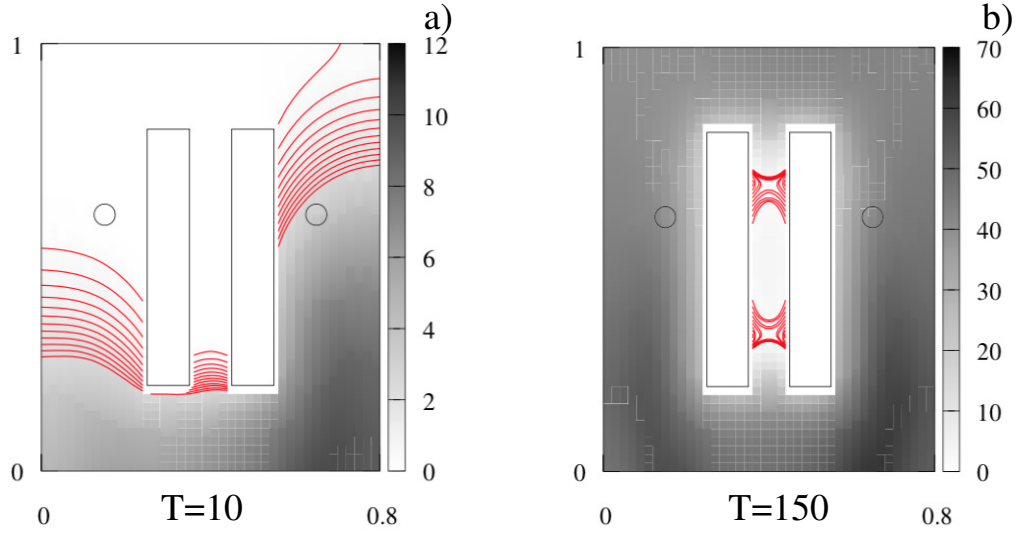


Figure 9: Spatial plots of τ for $\alpha = 1$, $\beta = 1$ and $\bar{U} = 0.01$ at two time instants: a) $T=10$, b) $T=150$.

spreading when we do not include τ in the model. In this section we want to assess the effects on the disease evolution when we increase the threshold \bar{U} including τ in the model. In the next simulation we use the same parameters set-up as in Case 2, except for the toxicity threshold that is set to $\bar{U} = 0.1$. We make this choice of the parameters since it is the one yielding a numerical steady state in which the brain is not completely damaged, thus possibly giving clinical insights on intervention measures against the disease.

The numerical outcomes of this simulation at the numerical stationary state are shown in Figures 10b) and 11b), respectively for the spatial plot of the degree of malfunctioning and the spatial plot of τ . Both pictures display a trend that is similar to that observed in Case 2 with a localization of the portion of damaged brain. However, since the threshold value $\bar{U} = 0.1$ for toxic u_2 is higher than the threshold value $\bar{U} = 0.01$ of Case 2, it happens that u_2 goes under \bar{U} much earlier than in Case 2. This finding translates into a spatial plot for the degree of malfunctioning

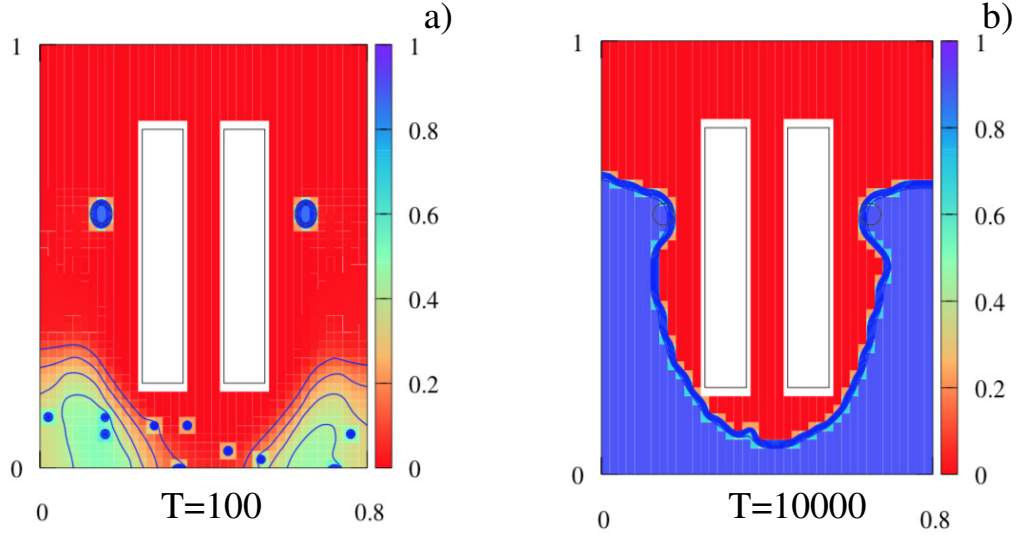


Figure 10: Spatial plots of the degree of malfunctioning for $\alpha = 10$, $\beta = 1$, $\bar{U} = 0.1$ and inculsion of τ at two times: a) $T=100$, b) $T=10000$.

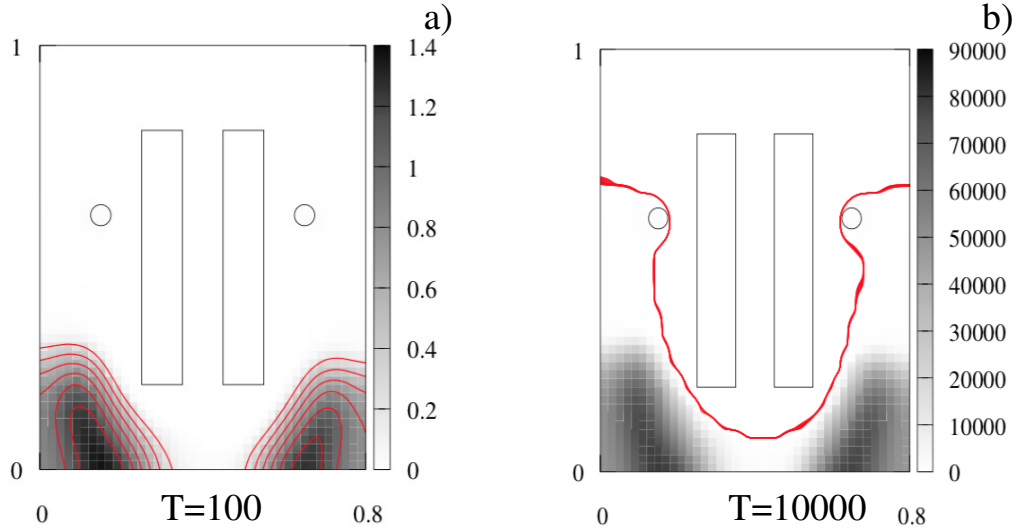


Figure 11: Spatial plots of τ for $\alpha = 1$, $\beta = 1$ and $\bar{U} = 0.1$ at two time instants: a) $T=100$, b) $T=10000$.

at equilibrium as in Figure 10 in which the brain is divided into two parts: the occipital part that is damaged and the frontal that is healthy.

4 Discussion

In this section we compare and discuss the numerical results of the simulated cases extensively described in Section 3 with the aim of pointing out the effects of varying the parameters focus of performed sensitivity analysis. The first insight we extrapolate from our analysis concerns the coagulation parameter α standing for the velocity at which the monomers and oligomers aggregate. We find out that setting α at least equal to 10 leads to a numerical stationary state of the system that does not correspond to a full damage of the brain, as in [2]. Depending on the remaining parameters of the model, we find different spatial localization of the damages,

ranging from small regions to larger ones, but in none of the cases considered the whole brain gets completely damaged. This result can have relevant clinical implications: it suggests the possibility of a drug therapy aiming to increase the aggregation rate of monomers and oligomers in order to control and localize the deterioration of the white matter. Another finding concerns the role of β : keeping fixed all other parameters, the higher the value of β we set, the lower is the resulting degree of malfunctioning of the brain (in both cases, with or without the inclusion of τ in the model). This is in agreement with the clinical evidence that an efficient clearance mechanism can control the brain damages produced by the combined effect of toxic $A\beta$ and τ . Finally, comparing the cases with and without τ and keeping all other parameters fixed, we clearly observe that the evolution of the disease is much faster and the damaged brain region larger when we include τ in the model. Looking at the spatial plots of the degree of malfunctioning this fact is evident. In conclusion, τ interacts with $A\beta$ accelerating the pathological dynamics of AD.

Acknowledgements

The authors would like to express their gratitude to MD Norina Marcello for many stimulating and fruitful discussions over several years.

B.F. and M.C.T. are supported by the University of Bologna, funds for selected research topics, by MAnET Marie Curie Initial Training Network and by GNAMPA of INDAM (Istituto Nazionale di Alta Matematica “F. Severi”), Italy.

M.B. thanks the project Beyond Borders (CUP E84I19002220005) of the University of Rome Tor Vergata. M.B. and V.M. acknowledge the MIUR Excellence Department Project awarded to the Department of Mathematics, University of Rome Tor Vergata, CUP E83C18000100006.

A.T. acknowledges support by the Italian Ministry of Education, University and Research (MIUR) through the “Dipartimenti di Eccellenza” Programme (2018-2022) – Department of Mathematical Sciences “G. L. Lagrange”, Politecnico di Torino (CUP:E11G18000350001) and through the PRIN 2017 project (No. 2017KKJP4X) “Innovative numerical methods for evolutionary partial differential equations and applications”. This work is also part of the activities of the Starting Grant “Attracting Excellent Professors” funded by “Compagnia di San Paolo” (Torino) and promoted by Politecnico di Torino. Moreover, A.T. acknowledges membership of GNFM (Gruppo Nazionale per la Fisica Matematica) of INDAM (Istituto Nazionale di Alta Matematica), Italy.

References

- [1] C. Ballard, S. Gauthier, A. Corbett, C. Brayne, D. Aarsland, and E. Jones. Alzheimers disease. *Lancet*, 377(9770):1019–1031, 2011.
- [2] M. Bertsch, B. Franchi, N. Marcello, M. C. Tesi, and A. Tosin. Alzheimer’s disease: a mathematical model for onset and progression. *Math. Med. Biol.*, 34(2):193–214, 2017.
- [3] M. Bertsch, B. Franchi, L. Meacci, M. Primicerio, and M. C. Tesi. The amyloid cascade hypothesis and alzheimer’s disease: a mathematical model. Submitted.
- [4] M. Bertsch, B. Franchi, M. C. Tesi, and A. Tosin. Microscopic and macroscopic models for the onset and progression of Alzheimer’s disease. *J. Phys. A: Math. Theor.*, 50(41):414003/1–22, 2017.
- [5] M. Bertsch, B. Franchi, M. C. Tesi, and A. Tosin. Well-posedness of a mathematical model for Alzheimer’s disease. *SIAM J. Math. Anal.*, 50(3):2362–2388, 2018.
- [6] C. Y. Chen, Y. H. Tseng, and J. P. Ward. A mathematical model demonstrating the role of interstitial fluid flow on the clearance and accumulation of amyloid β in the brain. *Math. Biosci.*, 317:108258, 17, 2019.

- [7] B. C. Dickerson, D. A. Wolk, and A. D. N. Initia. Biomarker-based prediction of progression in mci: comparison of ad signature and hippocampal volume with spinal fluid amyloid-beta and tau. *Alzheimers Dement*, pages 5–55, 2013.
- [8] G. G. Glenner and C. W. Wong. Alzheimers disease: initial report of the purification and characterization of a novel cerebrovascular amyloid protein. *Biochem Biophys Res Commun*, 120(3):885–890, 1984.
- [9] J. Götz, F. Chen, J. van Dorpe, and R. M. Nitsch. Formation of neurofibrillary tangles in p301l tau transgenic mice induced by $\alpha\beta_{42}$ fibrils. *Science*, 293(5534):1491–1495, 2001.
- [10] I. Grundke-Iqbal, K. Iqbal, Y. C. Tung, M. Quinlan, H. M. Wisniewski, and L. I. Binder. Abnormal phosphorylation of the microtubule-associated protein tau in alzheimer cytoskeletal pathology. *Biochem. Biophys. Res. Commun.*, 83(13):4913–4917, 1986.
- [11] J. L. Guo and V. M. Lee. Seeding of normal tau by pathological tau conformers drives pathogenesis of alzheimer-like tangles. *The Journal of Biological Chemistry*, 286(17):15317–15331, 2011.
- [12] L. W. Hung, G. D. Ciccotosto, E. Giannakis, D. J. Tew, K. Perez, C. L. Masters, R. Cappai, J. D. Wade, and K. J. Barnham. Amyloid- β peptide ($\alpha\beta$) neurotoxicity is modulated by the rate of peptide aggregation: $A\beta$ dimers and trimers correlate with neurotoxicity. *The Journal Neuroscience*, 28(46):11950–11958, November 2008.
- [13] J. J. Iliff, M. Wang, Y. Liao, B. A. Plogg, W. Peng, G. A. Gundersen, H. Benveniste, G. E. Vates, R. Deane, S. A. Goldman, E. A. Nagelhus, and M. Nedergaard. A paravascular pathway facilitates CSF flow through the brain parenchyma and the clearance of interstitial solutes, including amyloid β . *Sci. Transl. Med.*, 4(147):147ra111, 2012.
- [14] K. Iqbal, F. Liu, C. Gong, and I. Grundke-Iqbal. Tau in Alzheimer disease and related tauopathies. *Curr. Alzheimer Research*, 7(8):656–664, 2010.
- [15] Q.-L. Ma, F. Yang, E. R. Rosario, O. J. Ubeda, W. Beech, D. J. Gant, P. P. Chen, B. Hudspeth, C. Chen, Y. Zhao, H. V. Vinters, S. A. Frautschy, and G. M. Cole. β -amyloid oligomers induce phosphorylation of tau and inactivation of insulin receptor substrate via c-jun n-terminal kinase signaling: Suppression by omega-3 fatty acids and curcumin. *Journal of Neuroscience*, 29(28):9078–9089, 2009.
- [16] M. Meyer-Luehmann, T.L. Spires-Jones, C. Prada, M. Garcia-Alloza, A. De Calignon, A. Rozkalne, J. Koenigsknecht-Talboo, D. M. Holtzman, B. J. Bacskaï, and B. T. Hyman. Rapid appearance and local toxicity of amyloid- β plaques in a mouse model of Alzheimer’s disease. *Nature*, 451(7179):720–724, 2008.
- [17] T. A. Pascoal, S. Mathotaarachchi, M. Shin, A. L. Benedet, S. Mohades, S. Wang, T. Beaudry, M. S. Kang, J.-P. Soucy, A. Labbe, S. Gauthier, and P. Rosa-Neto. Synergistic interaction between amyloid and tau predicts the progression to dementia. *Alzheimer’s & Dementia*, 13(6):644 – 653, 2017.
- [18] Stephen William Scheff, Douglas A. Price, Frederick A. Schmitt, Steven DeKosky, and Elliott J. Mufson. Synaptic alterations in ca1 in mild alzheimer disease and mild cognitive impairment. *Neurology*, 68:1501–1508, 2007.
- [19] U. Sengupta, A.N. Nilson, and R. Kaye. The role of amyloid β oligomers in toxicity, propagation and immunotherapy. *EBioMedicine*, 6:42–49, 2016.
- [20] J.-M. Serot, J. Zmudka, and P. Jouanny. A possible role for CSF turnover and choroid plexus in the pathogenesis of late onset Alzheimer’s disease. *J. Alzheimer’s Dis.*, 30(1):17–26, 2012.

- [21] I.C. Stancu, B. Vasconcelos, D. Terwel, and I. Dewachter. Models of beta-amyloid induced tau-pathology: the long and folded road to understand the mechanism. *Mol Neurodegener.*, 9(51):1–14, 2014.
- [22] M. Vargas-Caballero, F. Denk, H. J. Wobst, E. Arch, C. M. Pegasiou, P. L. Oliver, O. A. Shipton, O. Paulsen, and R. Wade-Martins. Wild-type, but not mutant n296h, human tau restores $\alpha\beta$ -mediated inhibitory of ltp in tau in mice. *Front. Neurosci.*, 11(201), 2017.